UCRL- 94055
PREPRINT

$Sm^{2+} \rightarrow Nd^{3+}$ Energy Transfer in CaF_2

Stephen A. Payne
and
L. L. Chase

This paper was prepared for submittal to the
Journal of the Optical Society of America B.

February 3, 1986

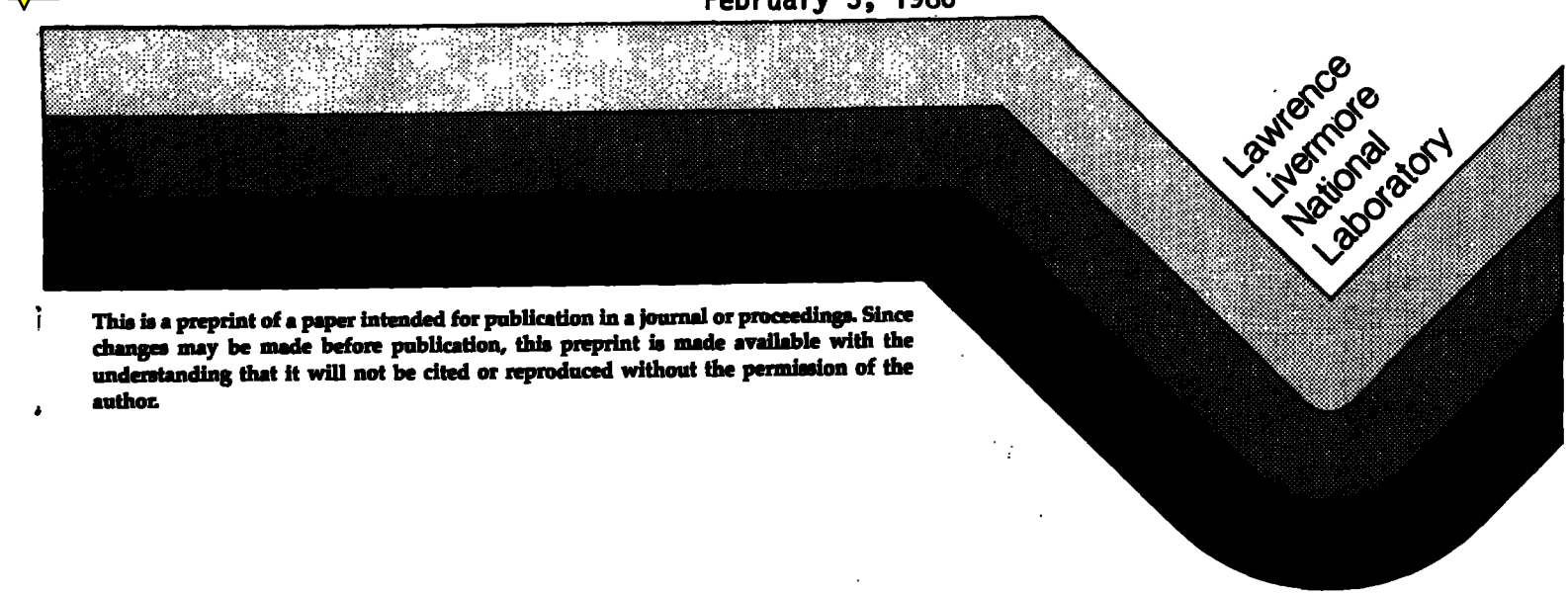

$Sm^{2+} \rightarrow Nd^{3+}$ Energy Transfer in CaF_2

Stephen A. Payne and L. L. Chase

Lawrence Livermore National Laboratory
University of California
Livermore, CA 94550

Abstract

We have measured the energy transfer efficiency of $Sm^{2+} \rightarrow Nd^{3+}$ in CaF_2 and have found that the transfer occurs through the dipole-dipole interaction. Our calculations of the efficiency from the emission and absorption properties of the Sm^{2+} and Nd^{3+} ions are in good agreement with those obtained from the Foerster-Dexter analysis of the emission transients. In addition, the comparison of the excitation and absorption spectra of co-doped samples quantitatively confirms that energy initially absorbed by Sm^{2+} is actually being converted into Nd^{3+} luminescence. Although efficiencies of 0.9 can be achieved with reasonable levels of Nd^{3+} doping, the Sm^{2+} luminescence begins to quench at temperatures >220 K. The selection of an optimal host for application to solid state laser systems is discussed in the light of the Sm^{2+} spectral characteristics and the need for good efficiency at room temperature.

1. Introduction

The study of energy transfer in inorganic phosphors continues to be an area of intense research because of its fundamental interest as a manifestation of long-range interaction of localized electrons in condensed matter, as well as for its practical utility in various devices. In this work we present our results for the CaF_2:Nd^{3+}, Sm^{2+} system, where we have found that $Sm^{2+} \rightarrow Nd^{3+}$ energy transfer is highly efficient at temperatures less than 220K. A possible application of this research lies in the development of more efficient solid state lasers. Since laser systems based on Nd-doped hosts are known to absorb less than 34% of the flashlamp light, efforts to increase the fraction of light absorbed provide a reasonable pursuit for system improvement.[1] However, the spectroscopic and dynamic properties of two different impurity ions must be well understood in order to select the proper host to optimize both the coupling with the flashlamp pump source, as well as the inter-ion energy transfer process. Here we explore the physics relevant to selecting the optimal laser host activated with Nd^{3+} and sensitized with Sm^{2+}. In this article we will consider the mechanism of $Sm^{2+} \rightarrow Nd^{3+}$ energy transfer. In addition we will address other problems such as the shift of the 4f-5d bands of Sm^{2+} with crystalline host, the quenching of Nd^{3+} luminescence by Sm^{3+}, the well-known effects of Nd^{3+} concentration quenching, and intra-ionic non-radiative decay of Sm^{2+}.

We now mention several recent studies to illustrate the diversity of interpretations of energy transfer problems. For example, Sibley and co-workers have examined $Eu^{2+} \rightarrow Mn^{2+}$ energy transfer in NaCl and $RbMgF_3$, and have concluded that the Eu^{2+} and Mn^{2+} ions preferentially form pairs, rendering the transfer rate anamolously high,[2,3] In contrast to these findings, other workers have found that the $Pb^{2+} \rightarrow Eu^{2+}$ transfer is of a radiative nature, i.e., photons emitted from Pb^{2+} are simply reabsorbed by the Eu^{2+} ions.[4,5] However, most studies conclude that the donor-acceptor distribution is random and that the energy transfer is of the dipole-dipole type described by Dexter.[6] Recent examples of this situation include

$Tb^{3+} \rightarrow Ce^{3+}$ transfer in YAG.[7] Another example involving the sensitization of Nd^{3+} luminescence by Cr^{3+} illustrates how a good understanding of the impurity ions lend to the selection of an appropriate host. We will discuss this case in detail below.

The development of Cr^{3+} sensitization of Nd^{3+} solid state lasers is informative both from a historical and a scientific perspective. The broad absorption bands of Cr^{3+} at 640 and 460 nm may be expected to efficiently absorb the flashlamp pump light.[8,9] In some materials, such as YAG, the lowest excited state of Cr^{3+} is the ^2E, hence the $^2E \rightarrow {}^4A_2$ transition is responsible for the emission. This makes the sensitization of Nd^{3+} by Cr^{3+} inefficient for two reasons: firstly, the Cr^{3+} emission band is fairly narrow resulting in poor spectral overlap with the Nd^{3+} absorption band, and secondly the emission lifetime of 1.53 ms was longer than that of Nd^{3+}, effectively increasing the overall emission lifetime of the laser crystal. Nevertheless, the application of simple crystal field (CF) theory provides an answer to these problems. The replacement of YAG with a host having a weaker CF would lower the $^4T_2$ state relative to the ^2E, and in so doing provide both broad-band emission and a short Cr^{3+} lifetime. Pruss, et.al., have pursued this with the use of the GdScGa-garnet (GSGG) host, where the emission lifetime is of the requisite duration, $\tau_{Cr} = 120\ \mu s < \tau_{Nd} = 250\ \mu s$, and transfer efficiencies as high as 0.86 have been achieved.[10] Other workers have shown that migration of energy among the donors (the Cr^{3+} ions) effectively increases the transfer efficiency.[11,12] Apparently GSGG:Nd^{3+}, Cr^{3+} has an overall conversion efficiency approximately twice that of YAG:Nd^{3+},[11] and this material has good potential for high-average-power laser applications.[13]

The CaF_2:Nd^{3+}, Sm^{2+} system offers many of the advantages of Cr^{3+}, and indeed several additional attractive features. The strong parity-allowed 4f→5d transitions in the visible and UV assure good absorption of broadband pump light but only require a fraction of the impurity concentration compared to Cr^{3+}. In addition the short emission lifetime of 1.4 μs and high transfer efficiency strongly

enhance the Nd^{3+} luminescent intensity without lengthening the Nd^{3+} emission lifetime. The short Sm^{2+} lifetime also serves to mitigate such potential problems as the excited state absorption of Sm^{2+} at Nd^{3+} emission wavelengths. Although the quantum efficiency of the Sm^{2+} emission intensity is known to decrease at temperatures greater than 220K rendering CaF_2 a poor host at room temperature, the present work serves to outline the potential advantages and disadvantages of a Sm^{2+} based sensitization scheme. We mention that the existence of $Sm^{2+} \rightarrow Nd^{3+}$ energy transfer was first noticed by Feofilov and co-workers many years ago, although they did not pursue this problem quantitatively.[14]

The rest of this paper is organized as follows: In Section 2 we will review the methods of the Foerster-Dexter (F-D) theory of energy transfer. We also perform some numerical computer calculations for the CaF_2 lattice to verify that we are working within the bounds of validity of F-D theory. In Section 3 we describe our experimental methods. In Section 4 the results are divided into three subsections, each representing a different way of calculating the $Sm^{2+} \rightarrow Nd^{3+}$ transfer efficiency. The discussion in Section 5 will be concerned with the physical properties of Sm^{2+} that may suggest an optimal laser host. Our concluding remarks are in Section 6.

2. Theory

Here we sketch the theory of sensitized luminescence developed by Foerster[15] and Dexter[6] (F-D) to provide the reader with a physical understanding of the energy transfer process, and also to check the validity of the approximations used with direct numerical calculations obtained with a computer.

In the F-D theory, Fermi's Golden Rule is used to describe the sensitizer (s) → activator (a) energy transfer rate with

$$P = (2\pi/\hbar)\rho \left| \int \Psi_I^* H_1 \Psi_F d\tau \right|^2 \qquad (1)$$

where $\Psi_I = \phi_s^e \phi_a^g$ and $\Psi_F = \phi_s^g \phi_a^e$, e and g stand for the excited and ground states, respectively, ρ is the density of states, and H_1 is the electric multipole-multipole interaction between the optically active electrons on the donor and acceptor atoms. For the electric dipole-dipole interaction, the transfer rate can be described as

$$P = \frac{R_o^6}{R^6 \tau_s} = \left(\frac{3}{4\pi}\right)\left(\frac{\pi c}{n}\right)^4 \frac{1}{R^6 \tau_s} \int \frac{F_s(E) \cdot \sigma_a(E)}{E^4} \, dE \qquad (2)$$

where F_s is the area-normalized emission spectrum of the sensitizer, σ_a is the lineshape of the activator absorption expressed in terms of the absolute value of the cross-section, τ_s is the sensitizer lifetime, and E is the photon energy. The parameter R_o is known as the critical radius, since when $R=R_o$ the rate of energy transfer is equal to the emission rate of the unperturbed donor. For the case of a narrow Gaussian absorption band at E_a and a wide Gaussian emission band at E_s we find

$$R_o^6 = \left(\frac{3}{4\pi}\right)\left(\frac{\pi c}{nE_a}\right)^4 \left[\frac{F_s(E_a) \cdot \sigma_a(E_a) \cdot (\Delta E_a^{1/2})}{F_s(E_s) \cdot (\Delta E_s^{1/2})}\right] \qquad (3)$$

where $\Delta E^{1/2}$ is the spectral half-width of the absorption or emission band, and the emission band normalization is included explicitly in the denominator. Equation 3 is the first method that we will use to calculate the critical radius (from which the overall efficiency can be obtained as will be shown later).

The temporal shape of the emission transient observed from a single sensitizer in the presence of activators can be written as

$$I_s = \exp\left(\frac{-t}{\tau_s}\right) \prod_{k=1}^{N_a} \exp\left[-P(R_k)t\right], \qquad (4)$$

where it is seen that a multiplicative exponential term is required for each of the N_a activators found at positions R_k around the sensitizer, and $P(R_k)$ is the rate constant for ion k. Of course, Eqn. 4 is missing a configurational average over all the different

possible environments that a sensitizer may see. The F-D theory is based on an approximation to (4) in which this configuration average is written as

$$I_s(t) = \exp\left(\frac{-t}{\tau_s}\right) \left[\sum_{k}^{N_L} W(R_k)\cdot\exp[-P(R_k)\cdot t]\right]^{N_a} \tag{5}$$

where we have summed over the N_L nearest lattice sites and we take this resulting sum to the power of the number of acceptors. $W(R_k)$ is the statistically averaged probability of occupying the site at R_k. Eqn. 5 can be understood by noting that each resulting term is of the form

$$\left\{W(R_k)\cdot W(R_\ell)\cdots W(R_m)\right\}\cdot\left\{\exp[-(P(R_k)+P(R_\ell)+\cdots+P(R_m))\cdot t]\right\}$$

This is essentially the product of the overall probability of the configuration occurring multiplied by the decay function of that configuration. However, since Eqn. 5 does permit configuations having more than one occupancy at a lattice site, we have the constraint that $C_a \ll 1$.

A closed-form solution for the transient decay of the sensitizers can be obtained through the additional approximation of a uniform density of acceptors around each donor

$$W(R) = 4\pi R^2 \frac{dR}{V}. \tag{6}$$

With the definition of a "critical concentration"

$$c_o = \left(\frac{4}{3}\pi R_o^3\right)^{-1} \tag{7}$$

the integration of Eqn. 5 over R yields[16]

$$I_s(t) = \exp\left(\frac{-t}{\tau_s}\right) \exp\left[-\sqrt{\pi}\,\frac{c}{c_o}\left(\frac{t}{\tau_s}\right)^{1/2}\right] \tag{8}$$

Thus if we plot

$$-\ln [I_s(t)] - \frac{t}{\tau_s} \quad \text{vs.} \quad \sqrt{t}$$

a line is obtained with a slope of $(\sqrt{\pi/\tau_s}) \cdot c/c_0$.

We can compare the results of Eqns. 4, 5 and 8 by producing plots of the nature described directly above. We have used a computer to numerically evaluate Eqns. 4 and 5 directly by summing over the lattice from the nearest neighbors at the [110] positions to the sites at [16,16,16] (using 1/48 of the lattice, as permitted by symmetry). 7500 random configurations were generated and then averaged for this Monte-Carlo simulation of Eqn. 4. On the other hand, Eqn. 5 assumes that the lattice sites are fractionally occupied at exactly the statistically averaged value. This approximation reduces the computer time to less than 1% of that used for Eqn. 4. We have found that the evaluation of Eqns. 4 and 5 and the actual F-D line deviate less than 2% from each other. The values $(R_0/R_L) = 4.35$ and the concentration $c = 0.5\%$ were used to obtain these results, where $R_L = 2.73$ Å is the F-F distance in CaF_2. These values are approximately the same as those obtained from our experiments, providing confidence in our use of F-D theory to analyze the data. For completeness, we mention that when $(R_0/R_L) \lesssim 1$ the discreteness of the lattice affects the sensitizer transfer rate such that the resulting curve is far from linear, and therefore the approximation of a uniform acceptor distribution (Eqn. 6) is no longer valid. Also, when $(R_0/R_L) \gtrsim 4$ and $c \gtrsim 3\%$ substantial curvature is seen in the Monte-Carlo plot. These situations have been discussed by a number of other workers,[17,18] although no computer calculations illustrating the nature and extent of the deviations from the F-D model have previously been carried out.

Upon examination of the F-D equation, we observe that the initial slope of the decay is predicted to be infinite. While this is not physically possible because of the existence of a minimum donor-acceptor distance, the transient does change very rapidly near t=0. Since our measuring apparatus does not resolve this initial fast decay, the data must be normalized at a time later than t=0, at $t=t_N$. Thus if we plot[7]

$$-\ln [I_s(t)/I_s(t_N)] - \frac{t-t_N}{\tau_s}$$

versus $\sqrt{t}$ we still obtain a line with a slope of $\sqrt{\pi/\tau_s} \cdot c/c_o$ and we are able to eliminate the time-resolution problems.

We discuss one other possible complication, which involves the migration of energy among the sensitizers. It is easy to see physically that this will accelerate the transfer rate since excited sensitizers located far from an activator will have the opportunity to move to a different sensitizer which may be located close to an activator. Because of the large oscillator strength of the Sm^{2+} f-d transition compared with the Nd^{3+} f-f transitions, $Sm^{2+} \rightarrow Sm^{2+}$ energy transfer may be significant even at relatively low Sm^{2+} concentrations. This effect may be approximately described with an exponential term of the form $\exp(-\bar{W}t)$, where $\bar{W}$ is proportional to both the activator and sensitizer concentration.[19]

Finally, once c/c_o is determined from the slope of the F-D line, we can calculate the efficiency, η, with[16]

$$\eta = \sqrt{\pi} \cdot \alpha \cdot \exp(\alpha^2) \cdot [1-\mathrm{erf}(\alpha)] \qquad (9)$$

where $\alpha = 1/2 \sqrt{\pi}\, c/c_o$ and erf is the error function. This concludes the discussion of our second method of calculating R_o. The third method is straightforward and will be discussed in context in Section 4.

3. Experimental

The experimental procedures employed are well-known methods and therefore are briefly discussed. The absorption spectra were obtained with a computer controlled Cary 17 spectrophotometer. A Molectron MY-34 YAG laser was used to pump a dye laser in order to provide excitation of the sample by ~10 nsec long pulses. Emission spectra were obtained by monitoring the signal from an S-1 photomultiplier tube (PMT) mounted at the exit slit of a Chromatix CT-103 monochromator with a gated boxcar integrator. The monochromator motor was stepped, and the boxcar output

was digitized, with a microcomputer. The emission lifetimes were recorded by connecting the PMT output to a Tektronix R7912 transient digitizer which provided time resolution as low as a few nanoseconds. A computer stored the transients so that they could be mathematically analyzed. The excitation spectra were obtained by monochromating the output of an Ealing 150 Watt xenon lamp. Before having the light impinge on the sample a small portion of the monochromated light was split off to serve as a reference. An interference filter isolated the 1.06 μm emission of the Nd^{3+} impurities which was monitored by the PMT. Lock-in techniques were employed to obtain a good signal-to-noise ratio, and the experiment was computer controlled. For all the above experiments, the temperature of the sample was controlled with an Air Products CS-202 closed-cycle helium refrigeration system. The single crystal samples were obtained from Optovac Corp.

4. Results

A. Absorption and Emission Spectra

The energy levels of Sm^{2+} and Nd^{3+} are schematically shown in Fig. 1, while the actual absorption and emission spectra are displayed in Fig. 2. We will investigate the process where Sm^{2+} is initially pumped to its excited state by the 4f→5d transitions, then subsequent energy transfer occurs via the Sm^{2+} emission and the Nd^{3+} absorption bands, and finally the Nd^{3+} ions emit the energy. The overall oscillator strength of the parity allowed f→d bands in CaF_2 is f=0.008.[20] As seen in Fig. 2, four major absorption bands are observed near 625, 420, 300 and 240 nm. Now, the 625 and 420 nm bands are known to shift to higher energy and the 300 nm band to lower energy in the spectra of the CaF_2-SrF_2-BaF_2 series. Since the crystal field is expected to get weaker with increasing cation size and the metal sites are cubally coordinated with fluoride ions, it is generally accepted that the excited states are derived from the $4f^5 5d(e_g)$ and $4f^5 5d(t_{2g})$ orbitals.[21,22] More recently, Yanase has suggested that the excited states responsible for the 625 and 420 nm bands arise from the coupling of the e_g electron with the ^6H and ^6F ($4f^5$) core states, respectively, and the 300 nm band from the t_{2g} electron with the ^6H state.[23]

The emission spectrum of Sm^{2+} is comprised mostly of a broad band at all temperatures, typical of that expected from the inter-configurational 5d→4f transition. $CaF_2:Sm^{2+}$ is unique in that the crystal field is sufficiently strong that the 5d level is the lowest excited state. In most other hosts the $^5D_0$ ($4f^6$) level is the lowest excited state and the low temperature emission consists primarily of a single sharp line. Perhaps most importantly, it is seen from Fig. 2 that the $CaF_2:Sm^{2+}$ emission overlaps the absorption bands of Nd^{3+}.

The sharp absorption features seen in Fig. 2 are due to the Nd^{3+} ions.[24] In particular we note that the Nd^{3+} bands located at 740 and 790 nm are crucial for the effective transfer of energy from Sm^{2+} to Nd^{3+}, as described in Section 2. Now, since Nd^{3+} replaces a Ca^{2+} ion, charge compensation is required somewhere in the crystal. The presence of a nearby charge compensator may be expected to reduce the symmetry from octahedral, thus providing electric dipole character to the normally parity-forbidden 4f-4f transitions. The lines observed for the Nd^{3+} luminescence spectrum shown in Fig. 2 indicate that the emission is occurring predominantly from C_{4v} sites, where an interstitial F^- resides on a neighboring empty Ca^{2+} site.[25] The situation is complicated further since it is known that the spectra of $CaF_2:Nd^{3+}$ change with concentration.[26] We have not observed the oxygen compensated sites seen by Toledano.[27] In passing, we mention that stimulated emission is typically obtained from the line at 1046.1 nm.[28]

At this point we know that the Nd^{3+} absorptions are of the forced electric dipole nature due to the charge compensation. We find for the 790 nm band of Nd^{3+} in Fig. 2 that the peak cross-section $\sigma_{Nd} = 2.3 \times 10^{-20}$ cm^2. Since the detector response was fairly flat over the range of the Sm^{2+} emission band, the data in Fig. 3 can be used in conjunction with Eqn. 3 to calculate that $R_0 = 13.0$Å, which corresponds to $c_0 = 0.43$ mole% of Nd^{3+} (see Eqn. 7). This is a reasonable concentration of Nd^{3+} to use in CaF_2. For a sample doped with $c=c_0=0.43$ mole%, the

$Sm^{2+} \rightarrow Nd^{3+}$ energy transfer efficiency would be 0.72 (using Eqn. 9). Of course there are a number of additional tests that are needed to confirm that the energy absorbed by Sm^{2+} is actually being converted into Nd^{3+} luminescence. However, the fact that the Nd^{3+} luminescence spectrum in Fig. 2 was obtained by exciting the Sm^{2+} band at 620 nm indicates that transfer is occurring. It should be noted that the dips in the Sm^{2+} emission spectrum in Fig. 2 caused by self-absorption by Nd^{3+} in the sample constitute a minor mechanism for energy transfer compared to the non-radiative F-D transfer.

B. Analysis of the Sm^{2+} Emission Transients

Here we analyze the emission transients of Sm^{2+} using the F-D theory described in Section 2. The four CaF_2 samples co-doped with Sm^{2+} and Nd^{3+} are listed in Table 1. Samples (a), (c) and (d) have progressively more Nd^{3+} with approximately the same amount of Sm^{2+}, while sample (b) has the same amount of Nd^{3+} as (a) but 11 times more Sm^{2+}. The emission transients observed from these four samples and that of a sample only doped with Sm^{2+} are shown in Fig. 3. Note that the intensity scale is logarithmic and that the t=0 intensity has been normalized to unity in each case. It is obvious that the decay rate increases from the 0% Nd^{3+} sample to the most heavily doped Nd^{3+} sample (see Table 1 and Fig. 3). These typical transients were obtained at T=100K. In order to obtain the value of c/c_0 we plot the transients as described in Section 2 by normalizing at t_N=0.2 μs after the fast laser excitation pulse. Examples of these plots are shown in Fig. 4 for T=10K. From the slopes of lines such as these and the concentration of Nd^{3+} listed in Table 1, the values of c_0 have been calculated for the temperatures 8, 100 and 200K (also in Table 1).

Now, c_0 is expected to be a constant for a particular host. While c_0 is reasonably consistent for samples (a), (c) and (d), sample (b) seems to deviate significantly. Therefore we use only the values of c_0 obtained from samples (a), (c) and (d), and defer discussion of sample (b) until later. The average c_0's calculated

in Table 1 indicate that there is little temperature dependence from 8K to 200K. Using Eqn. 7 the average R_o is found to be 11.9Å, in good agreement with the value of R_o=13.0Å determined from the overlap of the Sm^{2+} emission and Nd^{3+} absorption bands in Section 4A.

We can now use Eqn. (9) to calculate the energy transfer efficiency corresponding to the values of c/c_o. The c/c_o values have been determined using $t_N \approx 0.1$ to 0.6 μs. The results are shown in Fig. 5. With the exception of sample (b), the efficiencies remain fairly constant from 0 to 200K, at which point they begin to fall off. The explanation for this reduction in the transfer efficiency at T > 220K lies in the lifetime data of $CaF_2:Sm^{2+}$, displayed in Fig. 6. Since the luminescent efficiency of Sm^{2+} is quenching at temperatures greater than 200K, the data in Fig. 6 has been fit to the formula

$$\tau = \left[k_{rad} + A_{nr} \exp\left(\frac{-E_{nr}}{kT}\right) \right]^{-1} \qquad (10)$$

where $k_{rad}=(1.39\ \mu s)^{-1}$ is the radiative lifetime and $A_{nr}=2.55\times10^{11}\ s^{-1}$ and $E_{nr}=0.249$ eV are the non-radiative pre-exponential factor and activation energy, respectively. The drop in the luminescent quantum yield results in a decrease of the energy transfer efficiency since the inter-ionic transfer process must compete directly with the intra-ionic decay channel.

The deviation of sample (b) may be due to several causes. The higher concentration of Sm^{2+} may lead to clustering among the Sm^{2+} ions, or with the Nd^{3+} ions, rendering the impurity distributions non-statistical. Also the increase in the efficiency as a function of temperature seen in Fig. 5 may be caused by an increase in energy migration among the sensitizers (due to greater overlap of the absorption and emission bands of Sm^{2+}), as described in Section 2. We have estimated from Eqns. 3 and 7 a value of c_o=0.1% for Sm^{2+}-Sm^{2+} energy transfer at 200K using the measured overlap of the Sm^{2+} absorption and emission bands in

Fig. 2. This suggests that Sm-Sm transfer will play a significant role in the Sm-Nd transfer process for Sm^{2+} concentrations on the order of .1% or more.

C. Calculation of Transfer Efficiency using Excitation and Absorption Spectra

The energy transfer efficiency can be determined most directly, but perhaps not most accurately, by comparing the area of a selected Nd^{3+} band with that of a Sm^{2+} band, as obtained from an absorption spectrum and an excitation spectrum (resulting from monitoring Nd^{3+} luminescence). Figure 7 shows an example of such a comparison. The Nd^{3+} band utilized is at 575 nm while the Sm^{2+} band is at 625 nm. The excitation spectrum was taken by measuring the Nd^{3+} emission from 1040 to 1055 nm (see Fig. 2). At these wavelengths we are sure that there is no contribution from Sm^{2+} emission. The efficiency is then calculated with

$$\eta = [A(Sm,exc)/A(Sm,abs)]/[A(Nd,exc)/A(Nd,abs)] \qquad (12)$$

where A is the area of the Sm or Nd band derived from the absorption or excitation spectra, as indicated parenthetically. The results of these efficiencies are tabulated, along with those determined from the Sm^{2+} emission transients, in Table 2. Although the agreement is only fair, we note that the excitation spectra are not expected to be as accurate as the emission transients for determining transfer efficiency. Some problems with the former method involve the poor resolution of the excitation spectra, the possible depletion of the excitation source light due to narrow Nd^{3+} lines, the limited signal-to-noise ratio, the preferential monitoring of the luminescence of some Nd^{3+} sites, and the changes in the Nd^{3+} emission spectrum with temperature. Nevertheless the results do provide definitive confirmation that the energy being transferred from Sm^{2+} is being converted into Nd^{3+} luminescence (and not being non-radiatively depleted in some manner).

D. Nd^{3+}-Nd^{3+} and Nd^{3+}-Sm^{3+} Quenching

We have measured the Nd^{3+} emission lifetime at room temperature for the four co-doped samples as well as a sample doped only with Nd^{3+}. To do this we excited the Nd^{3+} band with 727.5 nm light and monitored the emission at 1045 nm. The lifetime obtained for a 0.2% Nd^{3+} sample was 1.1 ms, in agreement with the value reported by Kaminskii, et.al. for the C_{4V} Nd^{3+} sites.[29] They also showed that concentration quenching becomes significant at >0.3% Nd^{3+}. Our results are qualitatively similar since samples (a), (c) and (d) have lifetimes of 0.80, 0.60 and 0.15 ms (see Table 1 for the concentrations of Nd^{3+} and Sm^{2+}). Furthermore, sample (b) has a lifetime of 0.20 ms, despite the low Nd^{3+} concentration. This is explained by noting that the Sm^{3+} concentration is 4 times higher than in the other samples. From Fig. 2 it can be seen that the Nd^{3+} emission overlaps the Sm^{3+} absorption, which may therefore quench the activator luminescence. The possibility of this effect has been considered by Batygov, et.al.[30]

5. Discussion

The selection of an optimal host for a Sm^{2+} sensitized Nd^{3+}-doped solid state laser involves primarily two considerations: the non-radiative quenching of the Sm^{2+} emission, and the peak positions of the absorption and emission bands. We note that the Sm^{2+} absorption bands in CaF_2 are located between the Nd^{3+} bands, maximizing the spectral coverage of a flashlamp pump. CaF_2 may be quite useful for operation at temperatures below 250K, where the transfer efficiency is high. However, the luminescence is largely quenched at room temperature for CaF_2:Sm^{2+}. Although the other alkaline earth fluorides are also known to be Nd^{3+} laser hosts, the drop in luminescent quantum yield of Sm^{2+} is known to occur near 100K and 80K for the SrF_2 [31] and BaF_2 [32] hosts, respectively. Furthermore, the reduced CF of these hosts may be expected to result in a somewhat decreased overlap of the Sm^{2+} d-f emission with the Nd^{3+} absorption bands, and thus a reduced energy transfer rate. Thus the alkaline earth fluorides do not seem to be suitable hosts.

Although chlorides are not as useful laser hosts as are the fluorides and oxides, the properties of Sm^{2+} in these hosts may help provide an understanding of the non-radiative quenching process. It is notable that $SrCl_2:Sm^{2+}$ luminesces with good quantum efficiency at room temperature.[33] However the crystal field splitting of the Sm^{2+} 5d orbital is smaller for $SrCl_2$ than for CaF_2 and this results in the poor overlap of Sm^{2+} emission with the Nd^{3+} absorption bands. (Note that the Nd^{3+} bands also shift away from the Sm^{2+} emission.[34]) It is not well understood why the Sm^{2+} emission does not quench in $SrCl_2$, as it does in SrF_2, especially in the light of the similar absorption and emission spectra. Similarly Sm^{2+}:BaClF is known not to quench until temperatures near 600K are reached.[35] Apparently the presence of the chloride ion quite effectively increases the quenching temperature, even when it comprises only half of the anion lattice.

Selecting a host for a Sm^{2+} sensitized Nd^{3+} laser requires an understanding of the luminescence quenching. Non-radiative decay is normally considered within the single configuration coordinate model as described by Struck and Fonger.[36] They have shown that the magnitudes of the frequency and the offset of the totally symmetric vibrational coordinate for the ground and excited state energy surfaces can be used to predict the non-radiative relaxation rate. For the case of Sm^{2+} we may expect that non-radiative relaxation will occur via the low lying $4f^5 5d$ states to the $4f^6(^7F_J)$ ground states. It appears from their spectra that the 5d-4f configuration offsets of $SrF_2:Sm^{2+}$ and $SrCl_2:Sm^{2+}$ are similar, although the highest A_{1g} phonon peaks are quite different, being observed at 342[37] vs. 211 cm^{-1},[33] respectively. This is in qualitative agreement with the Struck and Fonger model since a smaller vibrational frequency implies a slower non-radiative rate. In addition, perhaps the trend of decreasing quenching temperature in going from CaF_2 to BaF_2 occurs because of an increase in the configurational offset. The lack of any vibrational fine structure in the absorption spectra of $BaF_2:Sm^{2+}$ at 4K is evidence of this effect.[21]

An additional complication exists in that, although some workers have claimed that the vibronic sidebands of Sm^{2+} can be completely described

by considering the linear and quadratic coupling terms for the A_{1g} vibrations,[37,38] several other authors have contended that the E_g vibrations are also active.[39,40] This poses the interesting question as to whether non-radiative decay might occur along a non-symmetric coordinate, such as that of E_g symmetry.

The above discussion has considered the non-radiative quenching of Sm^{2+} emission in terms of a curve crossing of the excited state potential energy surface with a ^7F_J ground state, be it along either the A_{1g} symmetric distortion or a non-totally symmetric coordinate. However, it is also possible that an ionization mechanism may account for the observed non-radiative processes. The formula of Pedrini, et.al.[41] can be used to calculate that the lowest $4f^55d$ level of Sm^{2+} lies at the bottom of the conduction band in BaF_2, while it is below it for both SrF_2 and CaF_2. Therefore the trend of decreasing quantum yield for the CaF_2-SrF_2-BaF_2 series may perhaps be understood in terms of a decrease of the activation energy needed to promote an electron to the conduction band. The photoconductivity measurements of Pedrini, et.al.[41] and the hole-burning experiments of Macfarlane and Meltzer[42] provide evidence for the ionization of Sm^{2+} in CaF_2. A forthcoming paper will consider this ionization mechanism in detail.[43]

6. Conclusion

The CaF_2:Sm^{2+}, Nd^{3+} system exhibits many of the properties ultimately required to successfully utilize Sm^{2+} sensitization for a Nd^{3+} doped laser host. The absorption bands are dipole-allowed and broad, and occur approximately between the Nd^{3+} bands. The short Sm^{2+} lifetime results in fast energy transfer, and the good overlap of the Sm^{2+} emission band with the Nd^{3+} absorption bands provides for efficient energy transfer. Since R_o=11.9Å for $Sm^{2+}\rightarrow Nd^{3+}$ transfer in CaF_2 while R_o=11.6Å for $Cr^{3+}\rightarrow Nd^{3+}$ transfer in GSGG[12], the efficiencies of the two systems are comparable. However the short Sm^{2+} lifetime diminishes potential problems associated with excited state absorption of Sm^{2+}, while the large oscillator strength of the f→d band greatly reduces the Sm^{2+} concentration necessary

(compared to Cr^{3+}). We have examined the energy transfer process by three independent methods to confirm that excitation of the Sm^{2+} ions is producing the expected increase in Nd^{3+} luminescence. We also numerically checked that Foerster-Dexter theory was valid within the range of the parameters we encountered. Since the Sm^{2+} luminescence quenches at T>220K, CaF_2 is not the optimal host. The ideal host must emit efficiently at room temperature, and also have a crystal field at the Sm^{2+} site similar to that encountered in CaF_2.

7. Acknowledgements

This research was performed under the auspices of the Division of Materials Sciences of the Office of Basic Energy Sciences, U.S. Department of Energy and Lawrence Livermore National Laboratory under Contract No. W-7405-Eng-48. We are indebted to W. F. Krupke, who suggested the possibility of rare earth sensitization by Sm^{2+}, and to Gary Wilke, who performed many of the measurements in this paper.

References

1. J. L. Emmett, W. F. Krupke and J. B. Trenholme, Sov. J. Quantum Electron. 13 (1), 1 (1983).

2. J. Rubio O., H. Murrieta S., R. C. Powell, W. A. Sibley, Phys. Rev. B31, 59 (1985).

3. M. D. Shinn and W. A. Sibley, Phys. Rev. B29, 3834 (1985).

4. J. G. Sole', C. Zaldo, J. Hernandez A., H. Murrieta S., and J. Rubio O., Solid State Commun. 54, 1021 (1985).

5. R. Capelletti, R. Cywinski, M. Manfredi and M. Solzi, Phys. Stat. Sol. (B) 128, 717 (1985).

6. D. L. Dexter, J. Chem Phys. 21, 836 (1953).

7. J. Shmulovich, G. W. Berkstresser and D. Brazen, J. Chem. Phys. 82, 1 (1985).

8. Z. T. Kiss and R. C. Duncan, Appl. Phys. Lett. 5, 200 (1964).

9. A. G. Avanesov, B. I. Denker, V. V. Osiko, V. G. Ostroumov, V. P. Sakun, V. A. Smirnov, and I. A. Shcherbakov, Sov. J. Quantum Electron. 12, 421 (1982).

10. D. Pruss, G. Huber, A. Beimowski, V. V. Laptev, I. A. Shcherbakov, Y. V. Zharikov, Appl. Phys. B28, 355 (1982).

11. E. V. Zharikov, N. N. Il'ichev, V. V. Laptev, A. A. Malyatin, V. G. Ostroumov, P. O. Pashinin, A. S. Dimenov, V. A. Smirnov, and I. A. Shcherbakov, Sov. J. Quantum. Electron. 13, 82 (1983).

12. E. V. Zharikov, V. V. Laptev, V. G. Ostroumov, Yu. S. Privis, V. A. Smirnov, and I. A. Shcherbakov, Sov. J. Quantum Electron. 14, 1056 (1984).

13. W. F. Krupke, M. D. Shinn, J. E. Marion, J. A. Caird and S. E. Stokowski, submitted to J. Opt. Soc. America.

14. Y. E. Kariss, M. N. Tolstoi and P. P. Feofilov, 18, 247 (1965).

15. T. Foerster, Z Naturforsh, 49, 321 (1949).

16. M. Inokuti and F. Hirayama, J. Chem. Phys. 43, 1978 (1963).

17. Y. K. Voron'ko, T. G. Mamedov, V. V. Osiko, A. M. Prokhorov, V. P. Sakun and I. A. Shcherbakov, Sov. Phys. JETP 44, 251 (1976).

18. V. P. Sakun, Sov. Phys. Solid State 14, 1906 (1973).

19. I. A. Bondar, A. I. Burshtein, A. V. Krutikov, L. P. Mezentseva, V. V. Osiko, V. P. Sakun, V. A. Smirnov and I. A. Shcherbakov, Sov. Phys. JEPT 54, 45 (1981).

20. V. A. Arkhangelskaya, M. N. Kiselyeva and V. M. Schraiber, Opt. Spectrosc. 23, 275 (1967).

21. D. L. Wood and W. Kaiser, Phys. Rev. 126, 2079 (1962).

22. P. P. Feofilov and A. A. Kaplyanskii, Opt. Spectrosc. 12, 272 (1962); A. A. Kaplyanskii and A. K. Przhevuskii, Opt. Spectrosc. 20, 577 (1966).

23. A. Yanase, J. Phys. Soc. Japan 42, 1680 (1977).

24. M. Zabkova, M. Svantnerand and V. Gasparik, Acta Phys. Slov. 29, 288 (1979).

25. C. A. Freeth and G. D. Jones, J. Phys. C Solid State 15, 6833 (1982).

26. Z. J. Kiss, J. Chem. Phys. 38, 1476 (1963); Y. K. Voron'ko, A. A. Kaminskii, and V. V. Osiko, Sov. Phys. JETP 22, 295 (1966).

27. J. C. Toledano, J. Chem. Phys. 57, 1046 (1972); ibid. 4468 (1972).

28. A. A. Kaminskii, JEPT Letters 6, 115 (1967).

29. A. A. Kaminskii, L. S. Kornienko and A. M. Prokhorov, Sov. Phys. JETP 21, 844 (1965).

30. S. Kh. Batygov, Yu. K. Voron'ko, M. V. Dmitruck, V. V. Osiko, A. M. Prokhorov and I. A. Shcherbakov in Spectroscopy of Laser Crystals with Ionic Structure, Proceedings of the P.N. Lebedev Institute 60, 31 (1974).

31. V. N. Baklanova, A. V. Bonch-Bruevich, and V. V. Ovsyankin, Opt. Spectrosc. 40, 404 (1976).

32. V. A. Bonch-Bruevich, and V. V. Ovsyankin, Sov. Phys. Solid State 17, 587 (1975).

33. J. D. Axe and P. P. Sorokin, Phys. Rev. 130, 945 (1962).

34. S. A. Payne and L. L. Chase, unpublished data.

35. A.S.M.M. Alan and B. DiBartolo, J. Chem. Phys. 47, 3790 (1967); J. C. Gacom, J. C. Souillat, J. Seriot and B. DiBartolo, Phys. Stat. Sol A39, 147 (1977).

36. C. W. Struck and W. H. Fonger, J. Luminesc. 10, 1 (1975).

37. V. A. Bonch-Bruevich, I. V. Ignatev, and V. V. Ovsyankin, Opt. Spectrosc. 44, 429 (1978).

38. V. A. Bonch-Bruevich, I. V. Ignatev and V. V. Ovsyankin, Opt. Spectrosc. 44, 296 (1978).

39. D. H. Kuhner, H. V. Lauer and W. E. Bron, Phys. Rev. B5, 4112 (1972).

40. S. A. Kazanksii, Opt. Spectrosc. 42, 179 (1977); A. V. Akimov, A. A. Kaplyanskii and S. P. Feofilov, Opt. Spectrosc. 54, 162 (1983).

41. C. Pedrini, D. S. McClure and C. H. Anderson, J. Chem. Phys. 70, 4959 (1979); C. Pedrini, F. Rogemond and D. S. McClure, J. Appl. Phys., to be published.

42. R. M. Macfarlane and R. S. Meltzer, Opt. Commun. 52, 320 (1985).

43. L. L. Chase, S. A. Payne and G. D. Wilke, submitted to J. Phys. C.

Figure 1. Schematic energy level diagram of Sm^{2+} and Nd^{3+} in CaF_2. The crystal field splitting is omitted. Three steps are illustrated: 4f→5d pumping of Sm^{2+}, the energy transfer that results from the Sm^{2+} 5d→4f transition and three Nd^{3+} upward transitions, and the emission of Nd^{3+} at the usual laser wavelength.

Figure 2. Absorption and emission spectra of sample (c) at T=200K with 0.39 mole% Nd^{3+} and 0.0087 mole% Sm^{2+}. On the left the broad bands are due to Sm^{2+} and the sharp features to Nd^{3+}. Sm^{2+} and Nd^{3+} emission spectra both resulted from excitation near 620 nm and were not corrected for the detector response.

Figure 3. Sm^{2+} emission transients at T=100K following an excitation pulse near 616 nm and detection at 720 nm. Sm^{2+} and Nd^{3+} concentrations for samples (a) through (d) are listed in Table 1.

Figure 4. Plots of $-\ell n[I_s(t)/I_s(t_N)]-(t-t_N)/\tau_s$ from which c/c_o is calculated using Foerster-Dexter theory for four Sm, Nd codoped samples (see text of Section 2 for theory and Table 1 for results).

Figure 5. Calculated energy transfer efficiency as a function of temperature for the four samples listed in Table 1 (see Section 2 for theory).

Figure 6. Emission lifetime of CaF_2:Sm^{2+} sample without Nd^{3+}. Solid line is a fit to Eqn. 10.

Figure 7. Absorption and excitation spectra of sample (c) with 0.39 mole% Nd^{3+} and 0.0087 mole% Sm^{2+} at T=200K. The Nd^{3+} emission from 1040 to 1055 nm was monitored for the excitation spectra. The efficiency is calculated using Eqn. 12 and the results are listed in Table 2.

Table 1.

Calculated values of c_o of Foerster-Dexter theory. The Nd^{3+} concentrations were determined with $\sigma(790\ nm)=2.3\times10^{-20}\ cm^2$, Sm^{2+} concentrations with $\sigma(620\ nm)=3.8\times10^{-18}\ cm^2$. Sample (b) was not included to determine the average c_o value. R_o was calculated with Eqn. 7.

Sample	Concentration (mole%)		c_o(mole%) 8K	c_o 100K	c_o 200K
	Nd	Sm			
a	0.16	0.0046	0.65	0.58	0.54
b	0.17	0.051	0.30	0.29	0.23
c	0.39	0.0087	0.53	0.53	0.51
d	1.1	0.0085	0.61	0.56	0.67
average C_o, samples a,c,d			0.60	0.56	0.57
average R_o(Å), samples a,c,d			11.7	12.0	11.9

Table 2.

Comparison of the $Sm^{2+} \rightarrow Nd^{3+}$ transfer efficiency determined from the absorption and excitation spectra (exc. + abs.), Section 4C, and from the method of Foerster and Dexter (F-D), Section 4B. The agreement is reasonable and the F-D method is more reliable.

Sample / T(K)	(a) Eff.		(c) Eff.		(d) Eff.	
	Exc. + Abs.	F-D	Exc. + Abs.	F-D	Exc. + Abs.	F-D
10	0.27	0.31	0.34	0.63	0.58	0.88
100	0.59	0.34	0.64	0.64	-	0.88
202	0.71	0.35	0.86	0.65	0.96	0.85
253	0.18	0.05	0.35	0.36	-	-
277	0.07	-	0.20	0.34	-	-
293	0.04	-	0.07	-	0.50	-

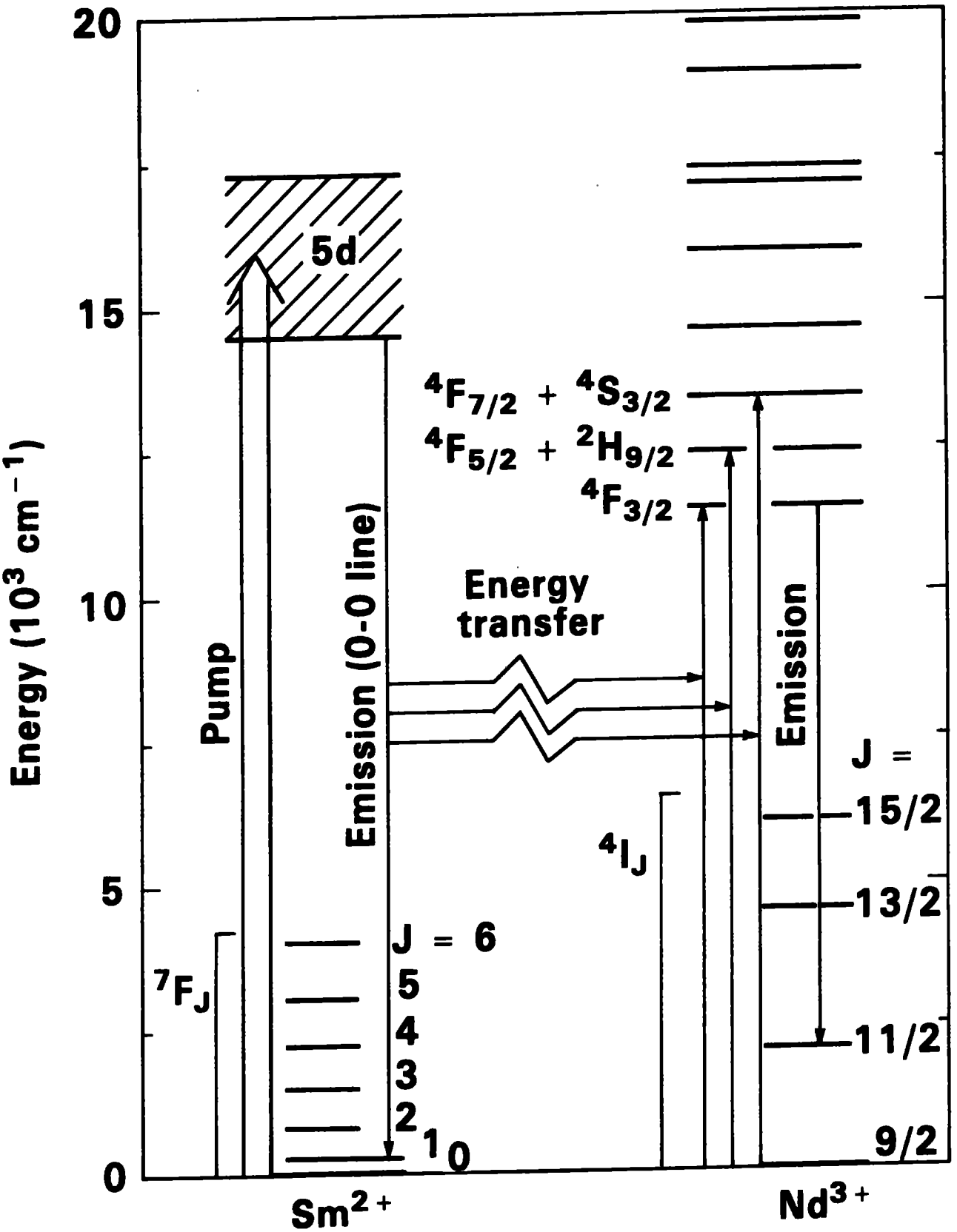
20
15
10
5
0
Energy (10^3 cm^{-1})
5d
Pump
Emission (0-0 line)
Energy transfer
$^4F_{7/2}$ + $^4S_{3/2}$
$^4F_{5/2}$ + $^2H_{9/2}$
$^4F_{3/2}$
^4I_J
Emission
J =
15/2
13/2
11/2
9/2
^7F_J
J = 6
5
4
3
2
1
0
Sm^{2+}
Nd^{3+}

Figure 1

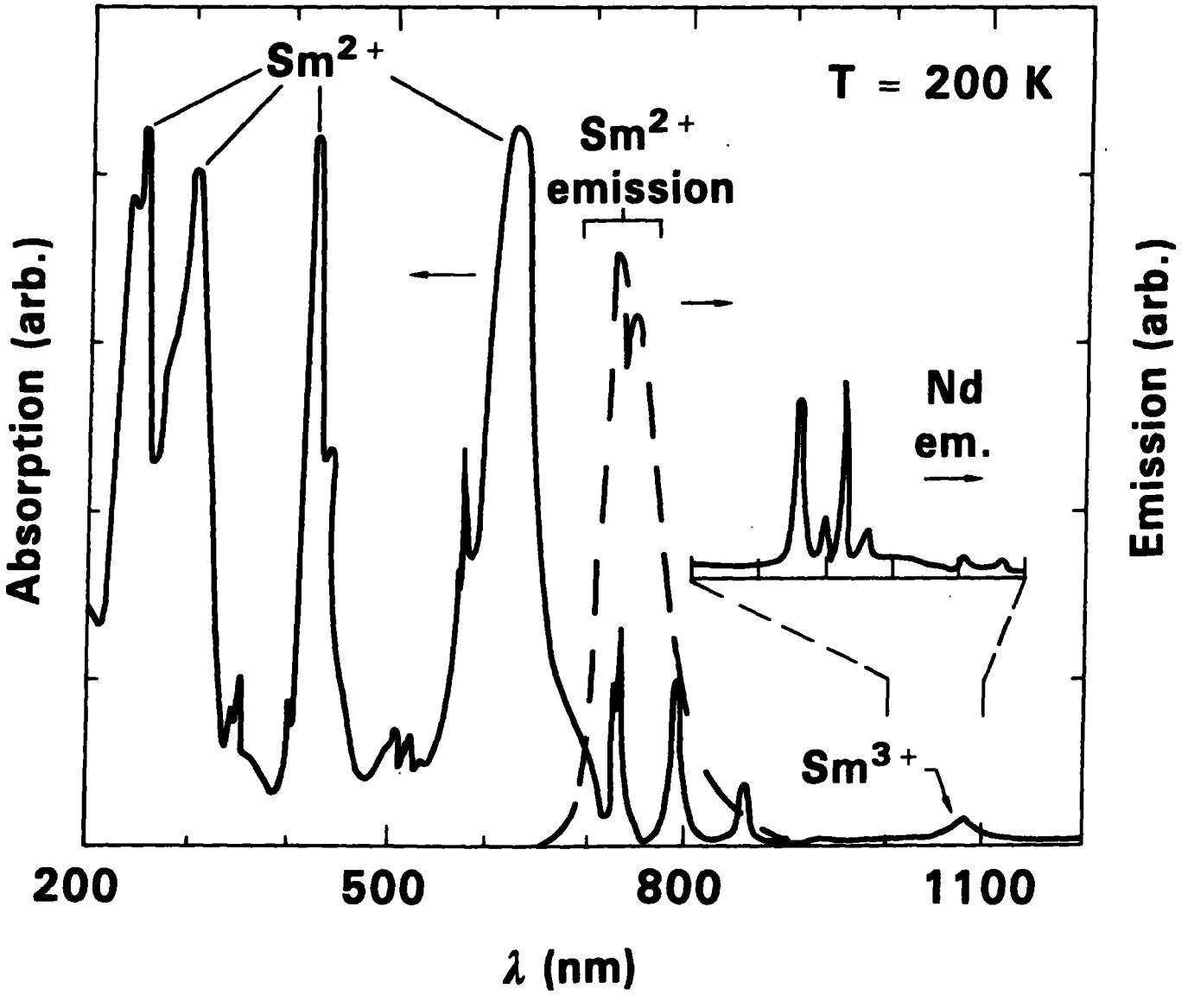
Sm2+
T = 200 K
Sm2+
emission
Nd
em.
Sm3+
Absorption (arb.)
Emission (arb.)
200
500
800
1100
λ (nm)

Figure 2

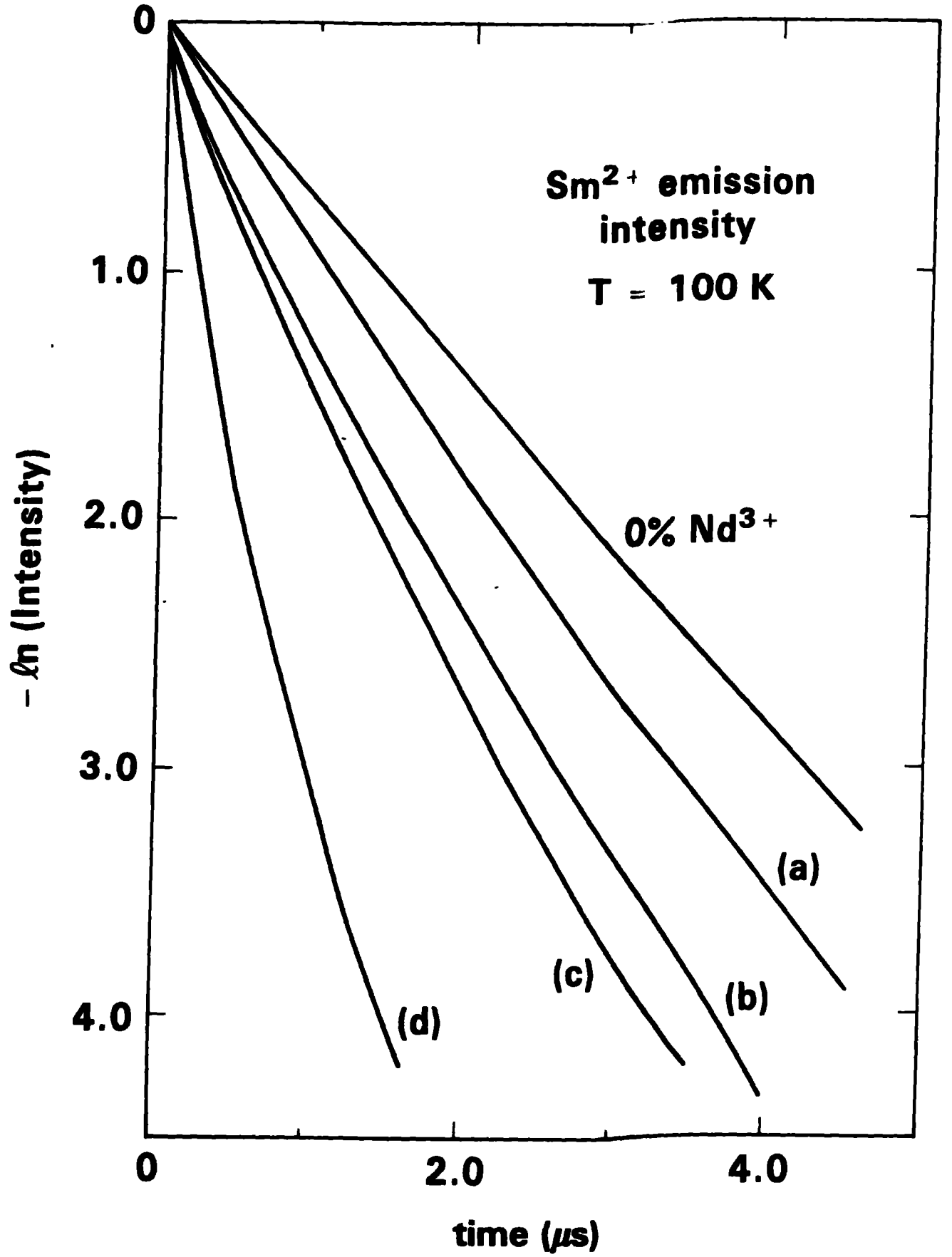
0
1.0
2.0
3.0
4.0
- ln (Intensity)
Sm2+ emission intensity
T = 100 K
0% Nd3+
(a)
(b)
(c)
(d)
0
2.0
4.0
time (μs)

Figure 3

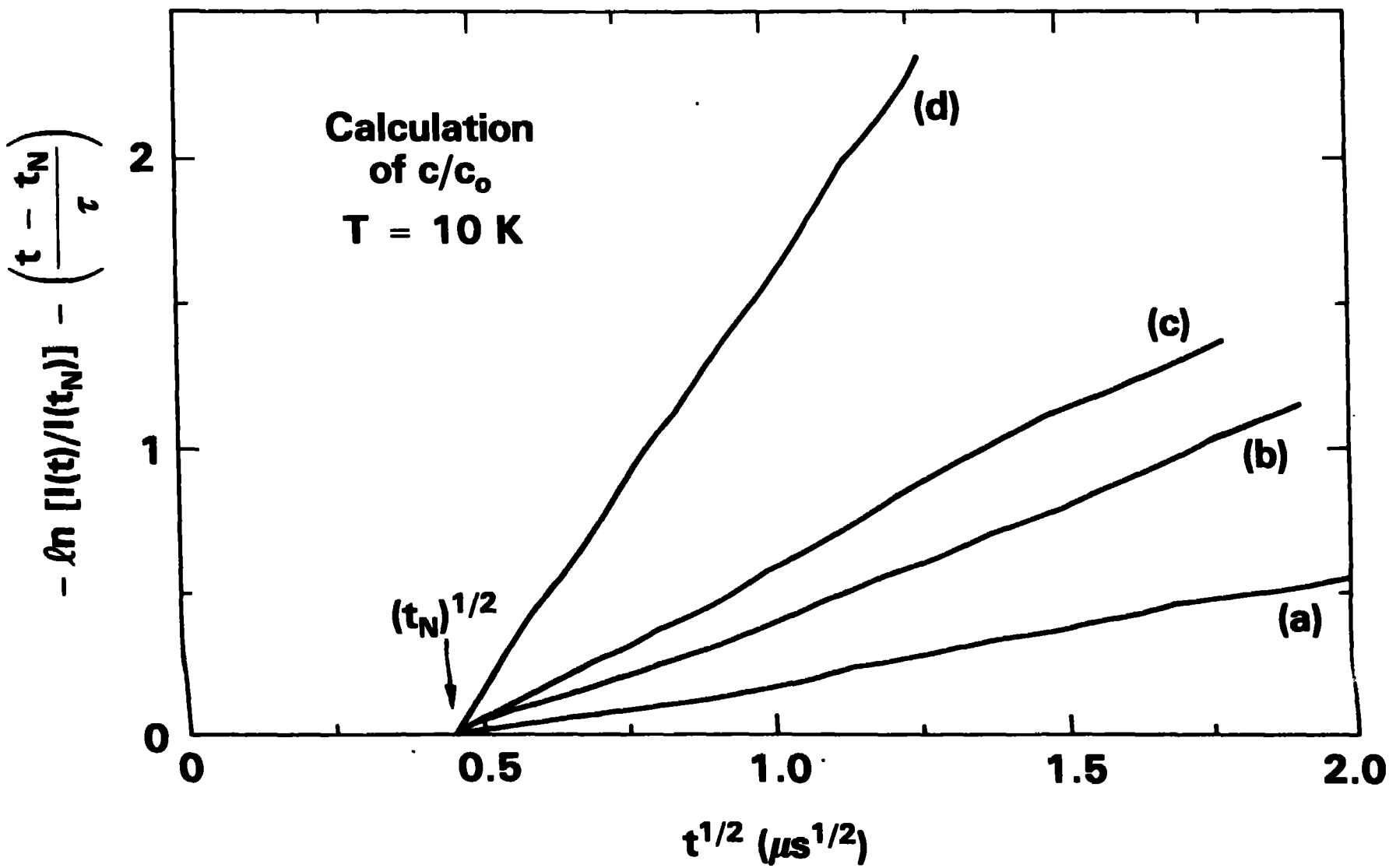
Calculation
of c/c$_o$
T = 10 K
(d)
(c)
(b)
(a)
(t$_N$)$^{1/2}$
$-\ln [I(t)/I(t_N)] - \left(\frac{t - t_N}{\tau}\right)$
t$^{1/2}$ (μs$^{1/2}$)
0
0.5
1.0
1.5
2.0
1
2

Figure 4

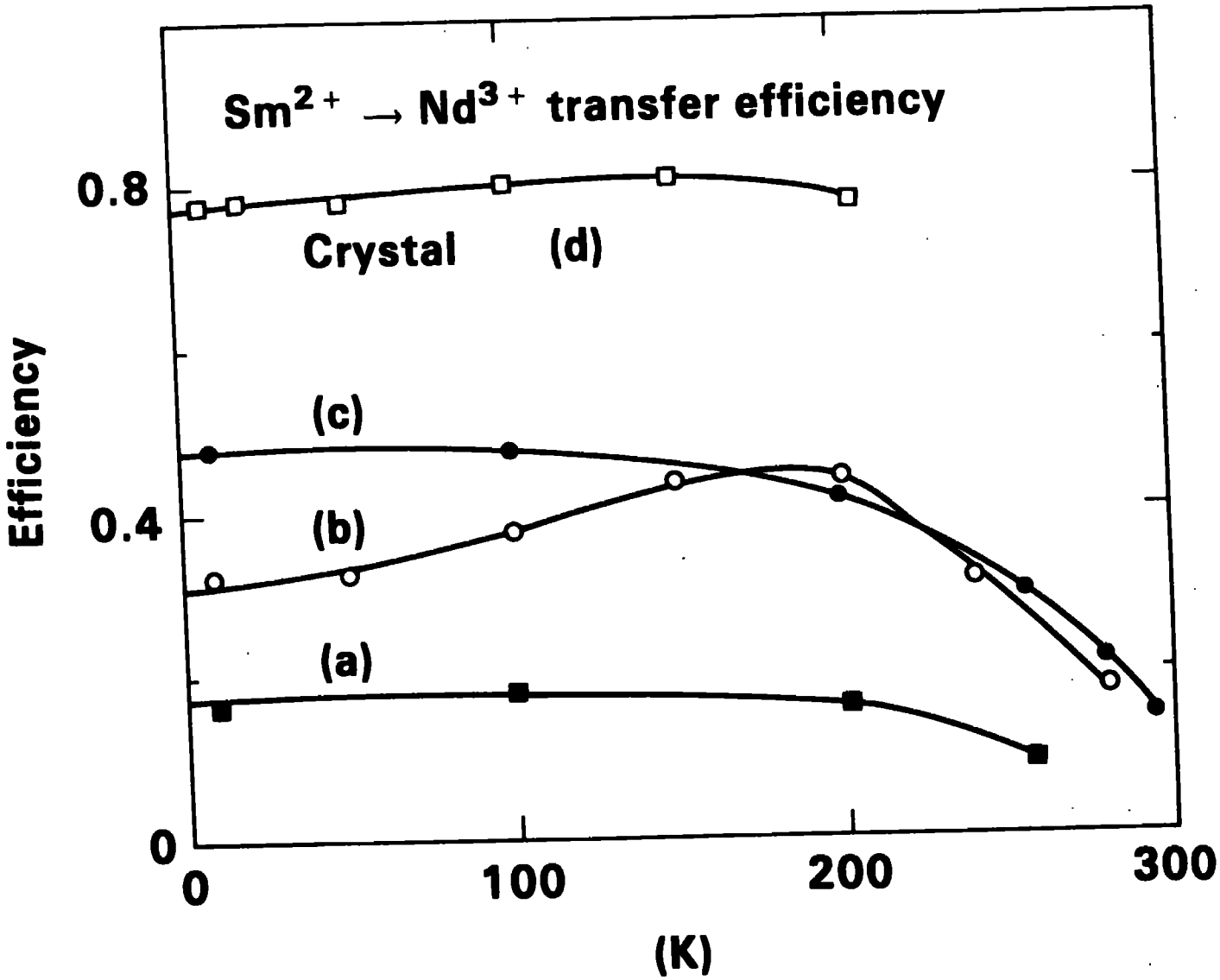
Sm2+ → Nd3+ transfer efficiency
0.8
Crystal (d)
(c)
(b)
(a)
Efficiency
0.4
0
0
100
200
300
(K)

Figure 5

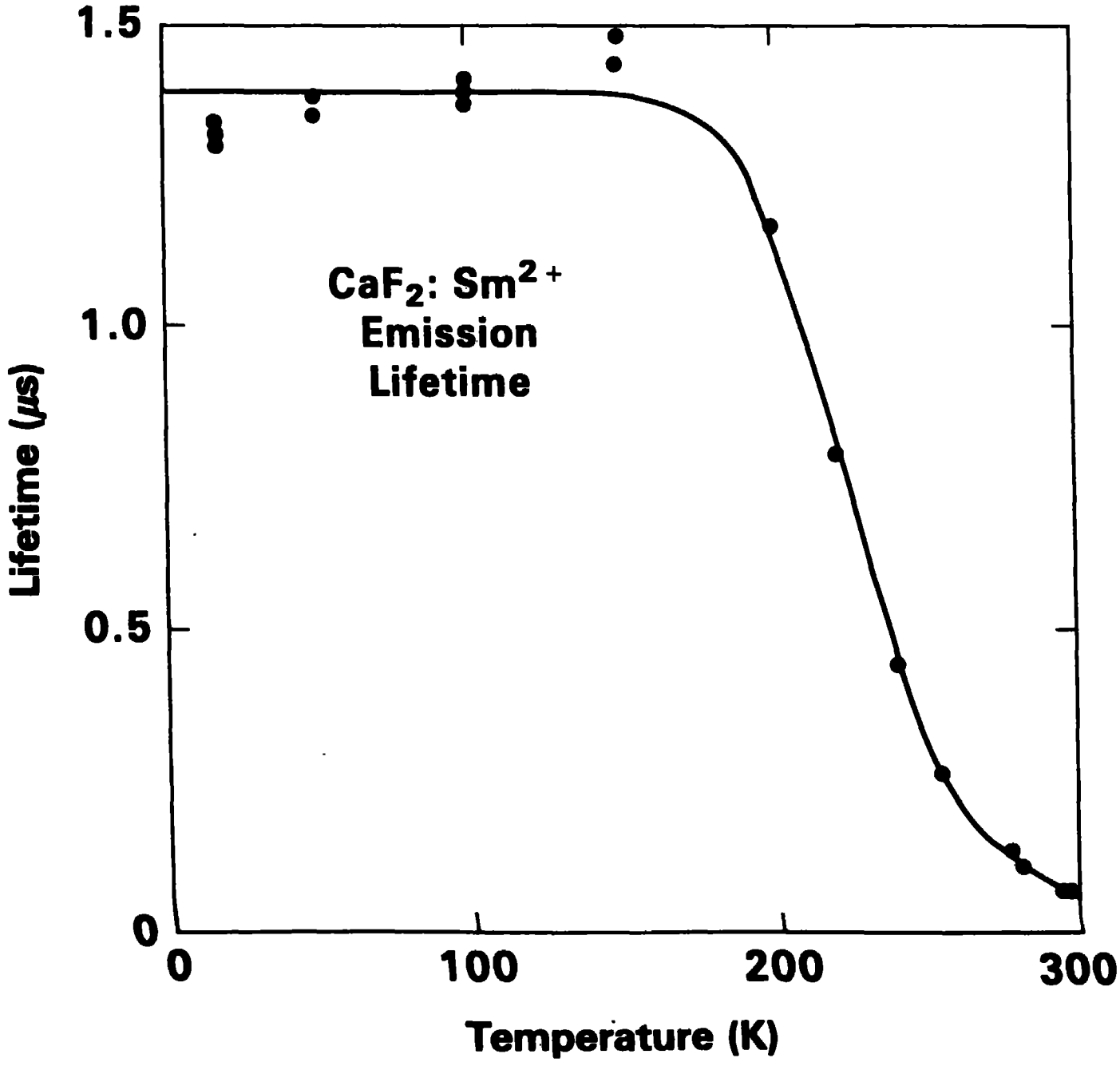
1.5
1.0
0.5
0
Lifetime (μs)
CaF2: Sm2+
Emission
Lifetime
0
100
200
300
Temperature (K)

Figure 6

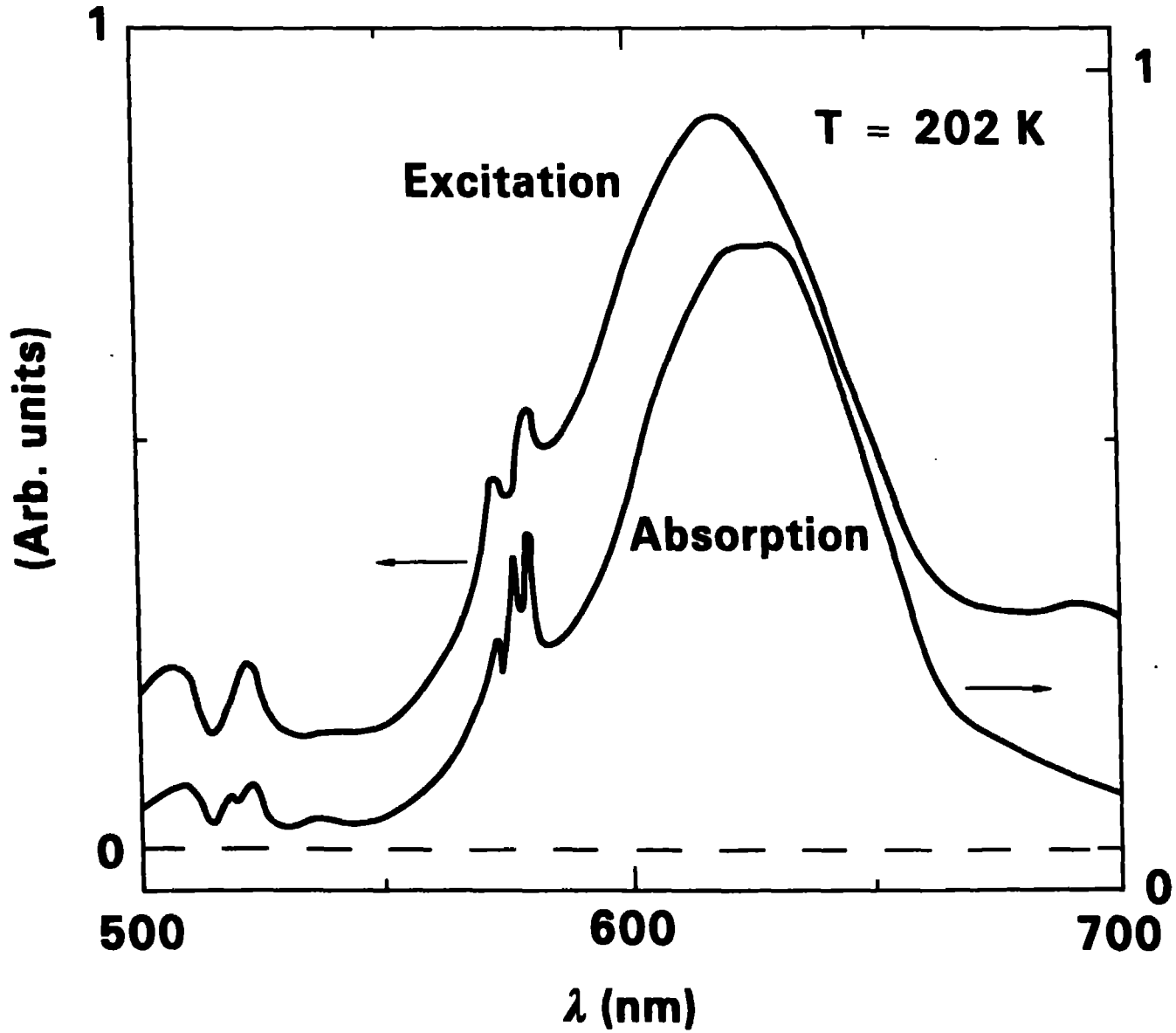

Figure 7